JOURNAL OF RAMAN SPECTROSCOPY
J. Raman Spectrosc. 2003; **34**: 642–650
Published online in Wiley InterScience (www.interscience.wiley.com). DOI: 10.1002/jrs.1045

JRS

Detection of single lipid bilayers with coherent anti-Stokes Raman scattering (CARS) microscopy

Eric O. Potma and X. S. Xie*

Department of Chemistry and Chemical Biology, Harvard University, Cambridge, Massachusetts 02138, USA

Received 6 January 2003; Accepted 31 March 2003

We investigated vibrational imaging of phospholipid bilayers with CARS microscopy. Single lipid membranes of supported bilayers, giant unilamellar vesicles and intact erythrocyte membrane are detected with the strong resonant signal of the C–H stretching vibration. In addition, it is shown that the CARS signal field of the lipids near the glass/water interface is amplified through mixing with the back-reflected non-resonant CARS field of the glass coverslip. Furthermore, interference effects between two separate bilayers are observed, allowing intermembrane distances to be determined beyond the diffraction-limited resolution of the microscope. Copyright © 2003 John Wiley & Sons, Ltd.

KEYWORDS: CARS microscopy; chemical imaging; phospholipid membranes

INTRODUCTION

Vibrational imaging techniques have the capability to map selectively molecular species based on the intrinsic properties of their chemical bonds. This is particularly useful for microscopic examinations of living cells under physiological conditions, omitting fluorescence labeling and fixation procedures. In addition, vibrational imaging is not prone to photobleaching that often complicates fluorescence microscopy. Spontaneous Raman microscopy has been applied to retrieve molecular information from complex biological systems such as single living cells,[1] human tissue[2] and individual chromosomes.[3] The key feature of the spontaneous Raman (confocal) microscope is that it yields detailed vibrational spectra from femtoliter volumes, from which molecular configuration and composition can be deduced. Because of the intrinsic weakness of the spontaneous Raman signal, long integration times are required. For a live cell, an image with appreciable contrast typically involves scanning times of more than 1 h.[1] Such long exposure times not only induce photo-damage to the system, but also limit the ability to follow the dynamics of live cells.

Coherent anti-Stokes Raman scattering (CARS) microscopy provides much stronger signals than spontaneous Raman microscopy.[4,5] CARS uses a pump and a Stokes beam, at frequencies ω_p and ω_S, respectively, to drive coherently a collection of Raman scatterers at the vibrational frequency $\omega_p - \omega_S$. This results in a strong CARS signal at the anti-Stokes frequency $2\omega_p - \omega_S$, in the phase-matched direction. Zumbusch *et al*.[5] adopted a collinear excitation geometry of tightly focused pump and Stokes beams and showed that in the forward direction (F-CARS) the phase-mismatch criterion ($\Delta k \approx 0$) is relaxed and strong CARS signals are produced. The combination of tight focusing and non-linear excitation allowed optical sectioning of thick samples, yielding 3D images. Various studies have demonstrated that this approach leads to image acquisition times as short as several seconds, allowing vibrational imaging of dynamic processes in cells.[6,7]

CARS is not background free; there exists a non-resonant signal due to the electronic response of the medium, particularly that of the solvent and the glass coverslip, which is virtually independent of the Raman shift $\omega_p - \omega_S$. To suppress the non-resonant background signal, polarization-sensitive detection can be employed.[8] Volkmer *et al*.[9] showed that the large phase mismatch in the epi-direction (E-CARS) can be used to detect the CARS signal of small objects, which is otherwise overwhelmed by the forward propagating background signal from the solvent. Furthermore, recent advances have shown the feasibility of multiplex-CARS microspectroscopy,[10,11] CARS correlation spectroscopy,[12,13] near-field CARS microscopy[14] and single-pulse CARS microscopy,[15] underlining the potential of the CARS approach to vibrational microscopy.

CARS microscopy has proven to be particularly successful in imaging lipid membranes. The high density of C—H bonds in the aliphatic chains gives rise to CARS signals

*Correspondence to: X. S. Xie, Department of Chemistry and Chemical Biology, Harvard University, 12 Oxford Street, Cambridge, Massachusetts 02138, USA.
E-mail: xie@chemistry.harvard.edu

Copyright © 2003 John Wiley & Sons, Ltd.

from organelle membranes, such as those of the nucleus and the mitochondrial network, well above background levels.[7] CARS microscopy thus offers a method for the rapid visualization of cellular phospholipid membranes under physiological conditions. Furthermore, CARS microspectroscopic investigations have revealed that detailed information on the lipid phase of the membrane can be obtained.[10,11] This opens up the possibility of investigating the existence of segregated phase domains in cellular membranes.[16]

In previous CARS studies, lipid signals were obtained from dense multilamellar vesicles or congested membrane structures in cells.[7,10,11] Here we explore the sensitivity of the CARS microscope for detecting unilamellar lipid membranes. It has been shown previously that Raman signals from single lipid bilayers on metal surfaces could be detected through surface-enhanced Raman scattering (SERS).[17] In this paper we demonstrate the single monolayer lipid sensitivity of CARS microscopy through visualization of supported lipid bilayers, unilamellar vesicles and red blood cell ghosts, without the requirement for metal surfaces. We show that mixing of the lipid CARS field with the CARS field from the glass substrate can be used to improve the sensitivity. In addition, an interesting interference effect is observed between two lipid bilayers. The experimental data are qualitatively explained by a theoretical analysis, the details of which can be found in the Appendices.

EXPERIMENTAL

Materials

The phospholipids 1,2-dioleoyl-*sn*-glycero-3-phosphocholine (DOPC) and 1,2-dioleoyl-*sn*-glycero-3-[phosphocholine-(1-glycerol)] (DOPG) were obtained from Avanti Polar Lipids. Millipore deionized water was used in all sample preparations. All other chemicals were purchased from Sigma Chemical.

Preparation of supported lipid bilayers

Multilamellar lipid layers were obtained by spreading 15 μl drops of a 5 mg ml^{-1} lipid in 9 : 1 chloroform–methanol solution on a glass coverslip. The sample was dried under vacuum for 4 h, immersed in 5 mM phosphate buffer solution, yielding layers with thickness of the order of several micrometers in addition to the formation of multilamellar vesicles.

Supported lipid bilayers were prepared through fusion of small unilamellar vesicles (SUV) on clean borosilicate coverslips, according to the procedure of Cremer and Boxer.[18] In brief, DOPC or 9 : 1 DOPC–DOPG was dissolved in 2 : 1 chloroform–methanol to give homogeneous solutions, after which the solvent was evaporated and dried under nitrogen. Lipid suspensions were made by diluting the lipid to a concentration of 2 mg ml^{-1} in 100 mM sodium phosphate buffer (pH 7.5). SUVs were formed by extruding the suspension through a 50 nm polycarbonate membrane filter (Avanti Mini Extruder). Coverslips (VWR) were cleaned by washing the substrates with ICN 7× detergent, rinsing thoroughly with deionized water and drying under a stream of nitrogen. Remaining organic structures were removed by baking the slips for 4 h at 400 °C. A 50 μl drop of the SUV solution was placed on the coverslip to promote spontaneous planar bilayer formation. The samples were washed and sealed by a second coverslip with a 150 μm spacer.

Preparation of giant unilamellar vesicles

Giant unilamellar vesicles (GUV) were obtained by the method of Akashi *et al*.[19] Dry lipid mixtures of 9 : 1 DOPC–DOPG were prepared by evaporating the solvent (2 : 1 chloroform–methanol) in small round-bottomed flasks. A solution containing 0.5 M sucrose that was prewarmed at 45 °C was added to dilute the lipids to a 1 mg ml^{-1} suspension. The flasks were placed in a 45 °C water-bath, which was cooled overnight to room temperature (21 °C), yielding a broad distribution of GUVs. Giant vesicles added to the solution above the supported bilayer sank rapidly to the bottom to form a close contact with the supported membrane.[20,21]

Preparation of erythrocyte ghosts

Human erythrocytes were collected by drawing ~50 μl of blood from a fingertip and diluted in aliquots containing 1 ml of heparinized buffer solution with a high osmolarity (~270 mOsm).[22] The erythrocytes were centrifuged for 3 min at 3000 rpm and the supernatant was removed from the pellet. The cells were washed three times before they were suspended on poly-L-lysine-coated glass coverslips. Under our excitation conditions, intact erythrocytes exhibit strong two-photon excited autofluorescence. To avoid the unwanted fluorescence of cellular constituents we first lysed the cells. To this end, the adhered cells were gently rinsed and exposed to ice-cold 5 mM phosphate buffer (pH 8.0). The hypotonic buffer causes the erythrocytes to lyse and the cellular content is released into the solution. The samples were kept close to 0 °C for 2 min, after which the cells were warmed in a resealing buffer (50 mM NaCl, 5 mM phosphate buffer, pH 8.0) to room temperature to allow resealing of the membranes during a 1 h incubation. The lysis and resealing procedure was repeated twice to remove all remaining hemoglobin from the cells. The erythrocyte ghosts appear as intact spherical vesicles when visualized with a phase-contrast light microscope.

CARS microscope setup

Two picosecond mode-locked Ti : sapphire lasers (Mira 900-P, Coherent) provide the pump (at frequency ω_p) and the Stokes (at frequency ω_s) beams. The Stokes laser was freely running whereas the pump laser was actively synchronized to the Stokes laser (Synchrolock, Coherent). Pulse jitters as low as 50 fs were obtained, which is almost two orders of magnitude shorter than the 3 ps temporal width of the pulses. Details on the light source can be found elsewhere.[23]

Copyright © 2003 John Wiley & Sons, Ltd.

JRS

In the E-CARS experiments, a laser repetition rate of 76 MHz was employed. The average power of the pump beam was 15–25 mW and the power of the Stokes beam was 15 mW. For the F-CARS measurements, each beam was pulse picked at a rate of 250 kHz with a Bragg cell. Average powers of the beams after pulse-picking were 0.3 mW for the pump and 0.1 mW for the Stokes laser, respectively. With the beam powers used, phospholipid membranes could be imaged for extended periods of time without any observable photo-induced damage.

The parallel polarized beams were expanded and combined on a dichroic mirror before they were directed into the inverted microscope (TE300, Nikon) with a 1.4 NA oil immersion lens (Plan Apo, Nikon). The backward-propagating E-CARS signal was separated from the incident light with a dichroic mirror, filtered by three bandpass filters (42-7336, Coherent) and focused on to a single photon avalanche photodiode (SPAD, SPCM-AQR-14, EG&G). In the forward direction, CARS radiation was collected with a 0.8 NA dry objective (LCM Plan, Olympus), spectrally isolated with bandpass filters and detected by an identical SPAD. The sample was scanned with a three-dimensional PZT stage scanner. The spatial resolution of the CARS microscope, as determined from 0.175 μm polystyrene bead measurements, was 0.27 μm in the lateral dimension and 0.66 μm along the axial coordinate.

RESULTS AND DISCUSSION

Figure 1 shows the geometry of CARS imaging experiments on lipid bilayers. For a single layer parallel to the glass interface [Fig. (1a)], equal amounts of CARS radiation are emitted in the forward and in the epi-direction.[9,24] The non-resonant background signal from the glass and the water is phase-matched in the forward direction and largely suppressed in the epi-direction. Planar bilayers are therefore best detected with E-CARS, because the signals are not accompanied by the non-resonant signal from the water bulk. In E-CARS, in addition to the lipid signal, a small fraction of the glass non-resonant signal is back-reflected from the surface, about 1% of the forward-propagating signal in our experimental settings.

If the lipid bilayer is oriented parallel to the optical axis, constructive interference in the forward direction yields strong signals for the F-CARS detection scheme and destructive interference renders virtually no signal in the epi-direction [Fig. 1(b)]. In this geometry, F-CARS is the method of choice for detecting the lipid bilayer. Both the signal from the membrane and the signal from the forward-propagating non-resonant background from the water bulk are detected with F-CARS.

The total CARS signal is composed of a resonant contribution $|\chi_r^{(3)}(\omega)|^2$, a non-resonant background $|\chi_{nr}^{(3)}|^2$ and a mixing term $2\mathrm{Re}\{\chi_r^{(3)}(\omega)\}\chi_{nr}^{(3)}$ (see Appendix 1). Here $\omega = \omega_0 - \omega_p + \omega_S$ indicates the detuning from the Raman resonance ω_0. Fig 2(a) displays the spectral characteristics of these contributions. The sum of these parts gives rise to the well-known CARS dispersive line shape with a dip on the high-energy side of the vibrational resonance, as depicted in Fig. 2(b) (solid line). This is a case in which the resonant signal is large. In the case of very weak resonant signals, $\mathrm{Re}\{\chi_r^{(3)}(\omega)\}\chi_{nr}^{(3)} >> |\chi_r^{(3)}(\omega)|^2$ and the CARS spectral line shape is dominated by the (dispersive) mixing contribution on a large non-resonant background,[10] as shown in Fig. 2(b) (dotted line). The strong non-resonant field can thus act as a source for amplifying the weak resonant CARS fields from the object, similar to signal amplification through heterodyne mixing.[25] In F-CARS, however, this mixing term might be buried in the noise of the overwhelming non-resonant signal from the water bulk. In E-CARS, the contribution from the water bulk is suppressed, but close to the coverslip, the back-reflected non-resonant signal from the glass (~1%) mixes with the signal field from the object. This represents a more favorable balancing of the non-resonant background and the mixing term. As a result, the signal amplification through mixing with the background is relatively more prominent. We refer to this mechanism as CARS amplification by heterodyne mixing. We also note that, for weak resonant signals, the magnitude of the dip on the high-energy side of the resonance

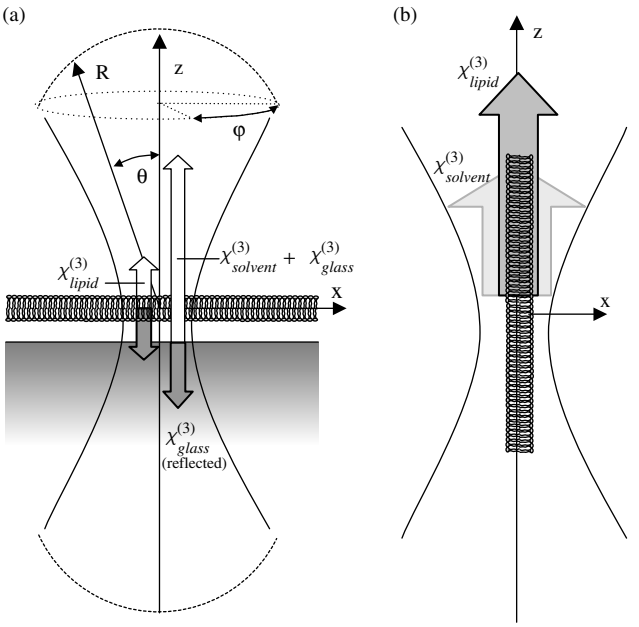

Figure 1. Schematic of the geometry of the CARS experiments. (a) Geometry of planar bilayer parallel to the glass surface. The gray arrows indicate the CARS field of the lipid and the glass (reflected) in the epi-direction, and white arrows the CARS field from the lipid, glass and solvent in the forward direction (not drawn to scale). (b) Geometry of bilayer parallel to the optical axis (*z*-axis). Arrows denote the CARS field from the lipid (dark gray) and the non-resonant signal field from the solvent (light gray) in the forward direction.

Copyright © 2003 John Wiley & Sons, Ltd.

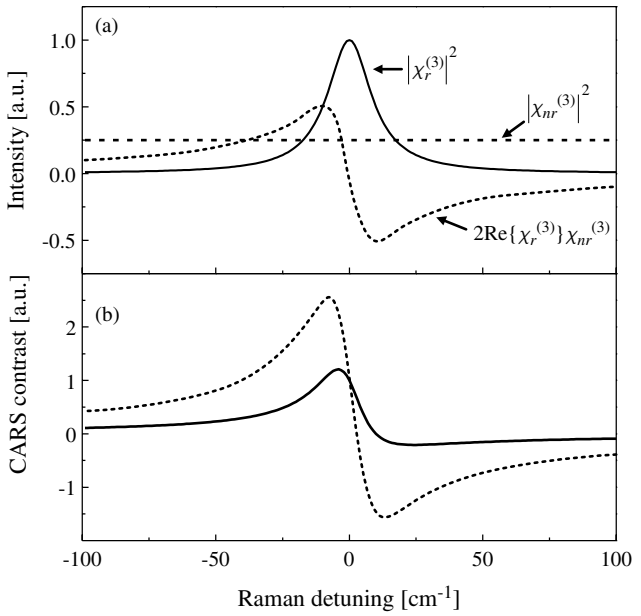

Figure 2. Illustration of the spectral characteristics of the CARS signal, modeled with a single Lorentzian vibrational line with $\Gamma = 10$ cm^{-1} and $a = 10$. (a) Contributions to the CARS signal, with the resonant part (solid line), a given non-resonant background (dashed) and the heterodyne contribution (dotted). (b) The CARS signal contrast for a weak non-resonant background with $|a/\chi_{nr}^{(3)}| = 20$ (solid) and for a stronger non-resonant background contribution of $|a/\chi_{nr}^{(3)}| = 5$ (dotted). In both curves $\varepsilon = 1$. See Appendix 1 for details. The non-resonant offset $|\chi_{nr}^{(3)}|^2$ has been subtracted. Note the more symmetrical dispersive lineshape in case of the stronger non-resonant background.

is expected to be comparable to the magnitude of the peak on the lower energy side of the resonance, i.e. $\mathrm{Re}\{\chi_r^{(3)}(\omega)\} \approx -\mathrm{Re}\{\chi_r^{(3)}(-\omega)\}$ as shown by the dotted line in Fig. 2b.

Lipid layers on glass supports

The E-CARS spectrum of multiple layers of DOPC on a clean coverslip is shown in Fig. 3. The corresponding Raman spectrum is given in the inset. A satisfactory fit to the spectrum was obtained by using a sum of eight Lorentzians (Table 1). The number of bands found below 3010 cm^{-1} complies with a previously given description of the Raman spectrum of DSPC,[11] a related phospholipid. The central wavenumbers and linewidths found from the Raman spectrum were used to describe the CARS spectrum (Appendix 1). Because of the presence of multiple bands, the overall CARS spectrum is much more complicated than the single band CARS spectrum plotted in Fig. 2(b). Nevertheless, characteristic features can be recognized. The CARS signal from the lipids clearly peaks above the back-reflected non-resonant signal from the coverslip, reaching its peak at 2849 cm^{-1}, the spectral region of the symmetric CH_2 vibrational mode. Above 2950 cm^{-1}, the CARS signal

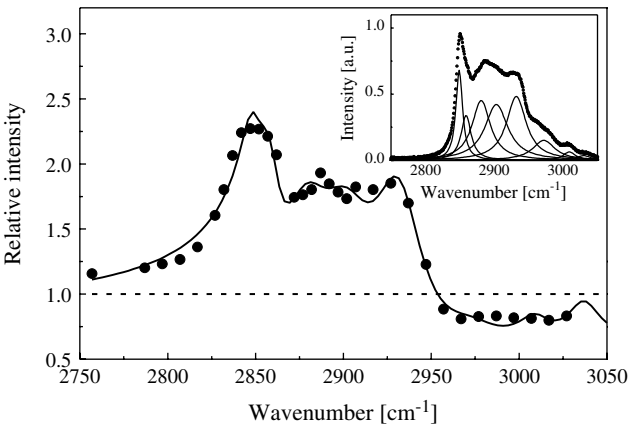

Figure 3. E-CARS spectrum of a multilamellar layer of DOPC on a clean glass coverslip. The pump beam was fixed at 13990 cm^{-1} while the wavenumber of the Stokes beam was varied. The spectrum is normalized to the background signal from the glass, which is indicated by the dashed line. The solid line is a fit to the data using Eqn (A4), normalized to the backscattered glass background $|r_{Fr}\chi_{glass}^{(3)}|^2$ and with $\varepsilon = 0.40$. Other parameters are given in Table 1. The inset shows the Raman spectrum of DOPC along with the eight Lorentzians used to describe the spectrum.

dips below the background signal from the glass, which is an indication that the lipid field mixes in a heterodyne manner with the glass field. From the fit [Eqn (A4)], it follows that ~40% of the back-reflected field from the glass efficiently mixes with the CARS field from the multiple phospholipid bilayers. It should be noted that the heterodyning with the non-resonant glass signal affects the spectral shape of the DOPC response. Qualitatively, it increases the lipid signal on the lower energy side of the spectrum whereas it gives rise to lower signals towards the higher energy side of the spectrum.

In order to study the sensitivity of the CARS microscope to single lipid membranes, supported lipid bilayers of DOPC

Table 1. Central wavenumbers (cm^{-1}), Raman linewidths and CARS amplitudes of the eight Lorentzians used in the fit to the normalized spectrum in Fig. 1, with the standard deviation of the last two digits of each fitting parameter in parenthesis

Wavenumber/cm^{-1}	FWHM/cm^{-1}	a_{CARS}
2849	11.4 (08)	1.43 (16)
2859	17.1 (03)	3.92 (21)
2881	32.0 (03)	6.38 (36)
2903	38.8 (04)	10.51 (42)
2932	34.5 (02)	14.35 (30)
2973	36.1 (07)	3.67 (65)
3009	20.4 (11)	2.88 (45)
3035	17.9 (20)	4.01 (44)

Copyright © 2003 John Wiley & Sons, Ltd.

JRS

were prepared. Figure 4(a) displays an E-CARS *xz*-scan of the supported bilayer with $(\omega_p - \omega_S)$ tuned to 2849 cm^{-1}. The signal is dominated by the back-reflected response of the glass. The lipid contribution at the glass interface amounts to 18% and can be visualized by subtracting the glass signal from the image, as shown in Fig. 4(b). The lipid bilayer shows up as a uniform layer in the lateral plane. The axial FWHM of the lipid signal is 0.63 μm, which is slightly smaller than the axial resolution of the microscope as determined with 0.175 μm polystyrene spheres. When the lasers are tuned to a Raman shift of 3000 cm^{-1}, a signal of reverse sign is seen at the glass/lipid interface. This confirms that the contrast observed is due to the lipid and that the mixing of the lipid signal field with the glass reflected field is relatively strong. Note that given the complex Raman spectrum of the phospholipid, the comparable magnitude of the peak (2849 cm^{-1}) and the dip (3000 cm^{-1}) is a mere coincidence rather than an expected feature.

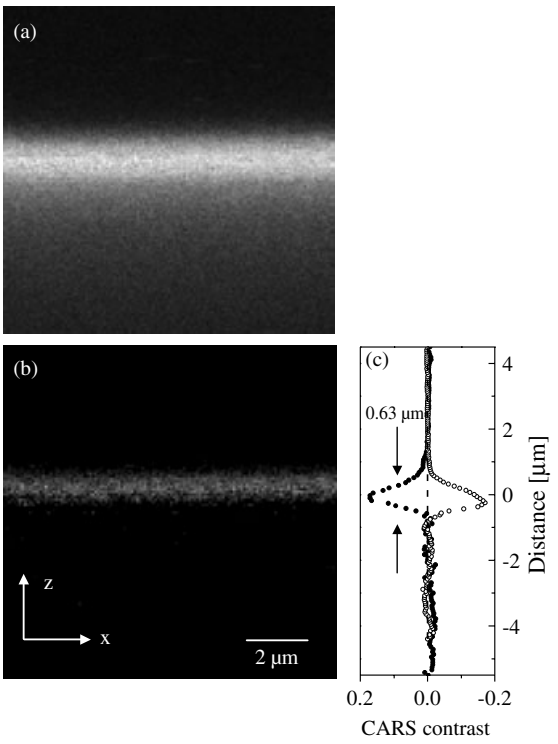

Figure 4. E-CARS image (*xz*) of a supported bilayer on a glass coverslip scanned axially through focus. (a) Total signal obtained at a Raman shift of 2849 cm^{-1} (pump at 13 990 cm^{-1}; Stokes laser at 11 141 cm^{-1}); (b) same image with the contribution from the glass subtracted; (c) one-dimensional projection of the lipid CARS contrast at 2849 cm^{-1} (solid circles) and 3000 cm^{-1} (open circles). The reverse contrast at the different wavenumbers arises because of the heterodyne mixing of the lipid CARS field with the glass CARS field. Images measure 10 × 10 μm, contain 128 × 128 points and the pixel dwell time is 2 ms.

Interference between two surfaces

To image lipid bilayers without interference with the glass signal, GUVs were added to the aqueous medium above the supported bilayer. In Fig. 5(a), a CARS image of the bottom of a giant vesicle above the glass interface is depicted. The strongest E-CARS signal from the GUV is observed from the lower part of the vesicle. In this region, the membrane is virtually parallel to the glass interface. More towards the side of the vesicle, the angle between the tangent of the membrane and the glass interface grows as the bilayer becomes more aligned with the optical axis. Because of the growth of the phase mismatch (see Fig. 1), the E-CARS signal from the membrane gradually decreases as the angle between the membrane plane and the interface increases.

The strength of the E-CARS signal from the membrane at 2849 cm^{-1} is ~6% compared with the non-resonant back-reflection from the glass. This is three times as weak as the heterodyned signal from the supported bilayer. Hence the heterodyning with the strong field of the glass support enhances the resonant signal from planar lipid layer at the

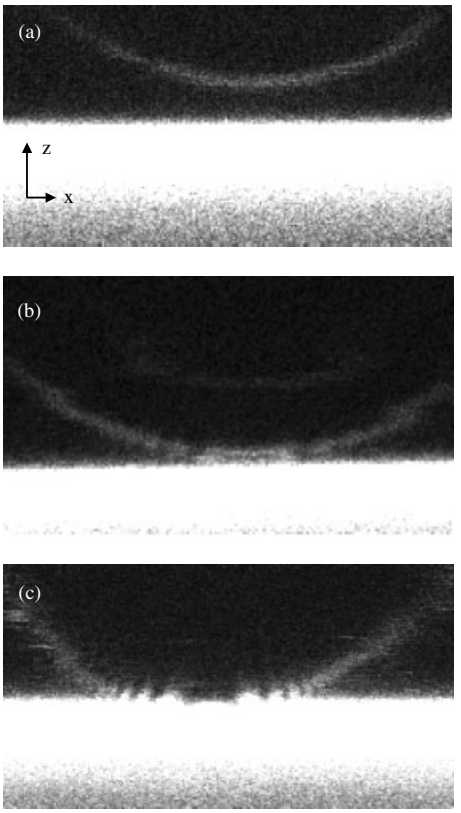

Figure 5. E-CARS images in the *xz* plane of a GUV close to a supported bilayer with different intermembrane separations: (a) ~3 μm (224 × 120 points); (b) ~0.5 μm (180 × 100 points); and (c) attached to the surface (240 × 160 points). Lasers are tuned to a Raman shift of 2849 cm^{-1}. Images measure 30 × 15 μm (x, z) with pixel dwell time of 2 ms. The length of the arrows is 2 μm.

Copyright © 2003 John Wiley & Sons, Ltd.

glass/water interface about threefold. When the GUV is examined at 3000 cm^{-1}, the signal essentially disappears. The membrane signal observed in Fig. 5(a) can thus be fully ascribed to the homodyne CARS signal from the membrane with a negligible contribution from reflections of the non-resonant water signal at the lipid/water interface. Assuming an area of 72.1 $Å^2$ per phospholipid molecule,[26] we estimate a total number of 4.4×10^6 active modes in the focal volume, which averages to 1.0×10^{-3} detected photons per second per mode under the current excitation and detection conditions.

When the lipid bilayer approaches the planar bilayer on the glass support within a distance comparable to the axial extent of the CARS excitation volume, the signal is composed of the field contributions from the supported lipid layer, the back-reflected glass field and the spatially separated GUV membrane. As a result, an interference pattern is observed, comparable to the interference effect in reflection interference contrast microscopy (RICM).[27] In Fig. 5(b), the GUV membrane is much closer to the planar layer than in Fig. 5(a) and the CARS signal is modulated as a function of the distance between the layers. This is more clearly illustrated at even shorter distances [Fig. 5(c)], where a strong modulation can be seen. The modulation results from the $-2k_{CARS}\Delta z$ phase difference between the layers. Up to four fringes can be discerned as the axial distance between the layers increases over a length scale defined by the focal volume. The axial distance between the bilayers can thus be determined with a precision beyond the axial resolution of the CARS microscope. This is shown in Fig. 6(a), which displays a one-dimensional cut through Fig. 5(c). Following the basic imaging properties of the CARS microscope as outlined in Appendices 2 and 3, a polynomial fit to the inter-membrane spacing could be found. The calculation is based on Eqn (A10) and includes the signal contributions of both membranes and the glass. As can be seen in the inset in Fig. 6(a), extrapolation of the calculated position of the upper membrane matches very well with its actual position. Figure 6(b) shows a simulation of the CARS signal close to the interface, using the same parameters as in Fig. 6(a). To visualize the contribution from the membrane only, the non-resonant back-reflection from the glass has been subtracted. The interference between the layers is clearly recognized. In concert with the experimental observations, the signal from the supported membrane appears about three times as strong as the signal from the GUV membrane because of the heterodyne mixing with the field from the glass substrate.

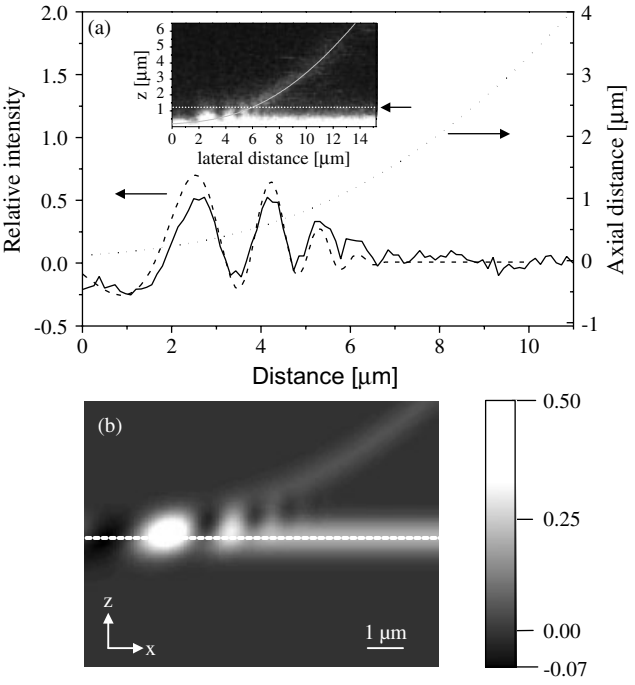

Figure 6. Interference fringes between two different lipid bilayers. (a) Lateral section through the fringes observed in Fig. 5(c). The dashed line represents a fit to the experimental data points based on Eqn (A10) and using a fourth-order polynomial to describe the intermembrane spacing. Resulting intermembrane distance is given by the dotted line. Inset: part of the image where the analysis was performed with the arrow indicating where the slice was taken. (b) Simulation of the image using Eqns (A10) and (A12) and the parameters found from the polynomial fit. The ratio $|\chi^{(3)}_{NR,lipid}/\chi^{(3)}_{R,lipid}|^2$ was set to 0.1, as estimated from an independent measurement of the non-resonant to resonant signal ratio, and $|\chi^{(3)}_{lipid}/(r_{Fr}\chi^{(3)}_{glass})|^2$ was fixed to 0.06. Signal levels are normalized to the glass signal, which has been subtracted for clarity. The dashed line refers to the glass/lipid interface. Image dimensions are 10×7 μm (x, z).

Natural membranes

So far, we have studied membrane structures prepared from purified phospholipids. Natural membranes, however, are composed of a variety of lipids that host membrane proteins. In addition, eukaryotic membranes contain cholesterol and are intimately associated with supporting protein structures and carbohydrates. In order to investigate the CARS signals from biomembranes, experiments on erythrocyte membranes were conducted. Erythrocyte ghosts were prepared to suppress signal contributions from the cell's interior. In Fig. 7, an F-CARS image taken in the equatorial plane of the erythrocyte vesicle is shown. The lasers are tuned to a Raman shift of 2845 cm^{-1}. The cells appear as spherically shaped, single-walled vesicles with a diameter of ~7 μm. The signal from the lipid bilayer peaks above the non-resonant signal of the surrounding water, confirming previous observations in living cells.[7] An interesting observation is that the signal is more than twofold stronger at the top and bottom of the vesicle image than on the left and right. When the polarization direction of both beams is rotated, this pattern rotates accordingly.[28] This suggests that there is on average a preferential orientation of the chemical C—H bonds, as is expected for the aligned acyl chains that make up the bilayer.

Copyright © 2003 John Wiley & Sons, Ltd.

JRS

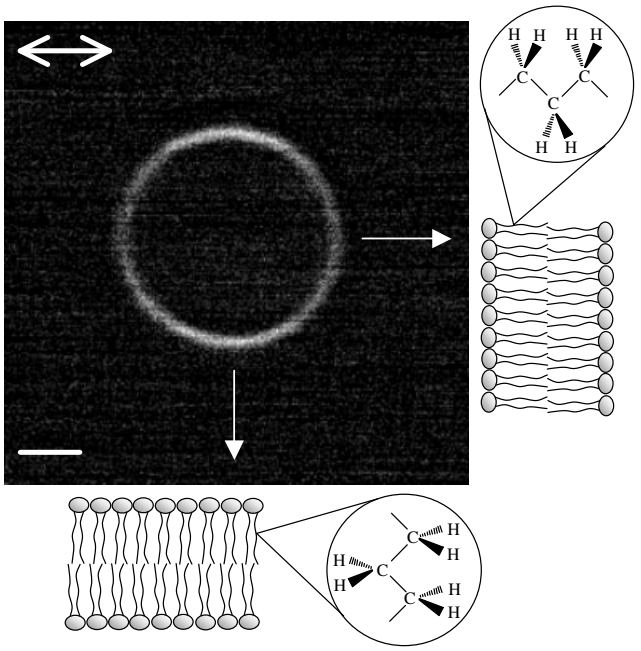

Figure 7. F-CARS image of erythrocyte ghost. Image was taken in the equatorial xy plane of the vesicle at a Raman shift of 2845 cm^{-1}. Arrows point toward the orientation of the bilayer, giving rise to a higher CARS intensity (top and bottom) when averaged C–H bond orientation is parallel with the incident beams (double arrow), and a lower CARS intensity (left and right) when C–H bond orientation is perpendicular to the incident polarization. Scale bar is 2 μm. Image size is 256 × 256 pixels and pixel dwell time is 1 ms.

An E-CARS image in the vicinity of the cell's bottom is given in Fig. 8(a). A pattern that is reminiscent of a ruffled membrane structure is observed. When the same cell is imaged at a Raman shift of 3000 cm^{-1}, a reversed pattern appears [Fig. 8(b)]. A one-dimensional cut through the figure, displayed in Fig. 8(c), shows that the signal at 3000 cm^{-1} is virtually the mirror image of the 2845 cm^{-1} signal. Similarly to the supported bilayers, this observation hints at a strong heterodyning of the lipid CARS field with the nonresonant signal field from the substrate.

CONCLUSION

We examined the CARS signal from single lipid bilayers. Planar membrane structures perpendicular to the optical axis are clearly visualized free of the non-resonant signal from water with E-CARS. Close to the glass surface, the back-reflected signal from the glass coverslip can be used to enhance the signal from the membrane threefold. This heterodyne amplification effect is also observed from natural membranes and may prove useful for increasing the image contrast of other sample structures close to the glass support as well. In addition, the interference of the CARS fields from two spatially separated sources can be used to determine

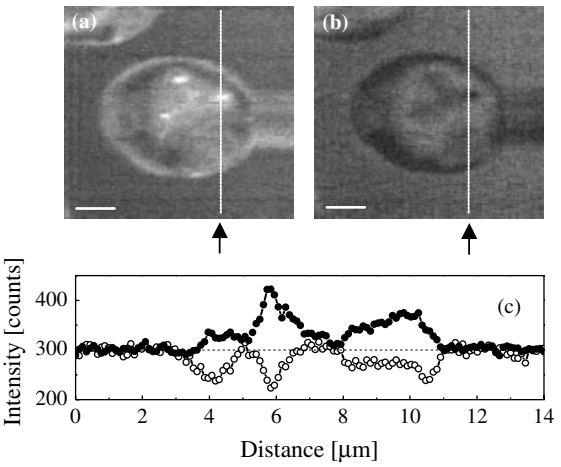

Figure 8. (a) E-CARS images of an erythrocyte ghost taken in the focal plane close to the glass/water interface (Raman shift 2845 cm^{-1}). The scale bar is 2 μm. Image is recorded with 128 × 128 pixels and a pixel dwell time of 2 ms. (b) Same ghost imaged at 3000 cm^{-1}. (c) One-dimensional cross-sections through (a) [solid circles, taken at the arrow in (a)] and (c) [open circles, taken at the arrow in (c)]. Note the reverse contrast.

their relative axial distance with a precision greater than the resolution of the microscope. These studies indicate that CARS microscopy is a highly sensitive approach to examine unilamellar membranes. The high sensitivity should allow images to be generated at higher scanning rates, offering promise for cellular imaging and resolving dynamic processes such as lipid segregation in unstained membranes.

Acknowledgments

This work was supported by an NIH grant (GM62536-01). We thank C. Evans for help with some of the experiments and J.-X. Cheng for helpful discussions. J. Pawley is acknowledged for pointing out the erythrocyte model system to us. E.O.P. acknowledges financial support from the European Molecular Biology Organization (EMBO).

REFERENCES

1. Puppels GJ, Olminkhof JHF, Segers-Nolten GMJ, Otto C, de Mul FFM, Greve J. *Exp. Cell Res.* 1991; **195**: 362.
2. Shafer-Peltier KE, Haka AS, Fitzmaurice M, Crowe J, Myles J, Dasari RR, Feld MS. *J. Raman Spectrosc.* 2002; **33**: 552.
3. Puppels GJ, de Mul FFM, Otto C, Greve J, Robert-Nicaud M, Arndt-Jovin DJ, Jovin TM. *Nature (London)* 1990; **347**: 301.
4. Duncan MD, Reintjes J, Manuccia TJ. *Opt. Lett.* 1982; **7**: 350.
5. Zumbusch A, Holtom GR, Xie XS. *Phys. Rev. Lett.* 1999; **82**: 4142.
6. Potma EO, de Boeij WP, van Haastert PJM, Wiersma DA. *Proc. Natl. Acad. Sci. USA* 2001; **98**: 1577.
7. Cheng J-X, Jia YK, Zheng G, Xie XS. *Biophys. J.* 2002; **83**: 502.
8. Cheng J-X, Book LD, Xie XS. *Opt. Lett.* 2001; **26**: 1341.
9. Volkmer A, Cheng J-X, Xie XS. *Phys. Rev. Lett.* 2001; **87**: 023 901.
10. Müller M, Schins JM. *J. Phys. Chem. B* 2002; **106**: 3715.
11. Cheng J-X, Volkmer A, Book LD, Xie XS. *J. Phys. Chem. B* 2002; **106**: 8493.

Copyright © 2003 John Wiley & Sons, Ltd.

12. Hellerer T, Schiller A, Jung G, Zumbusch A. *ChemPhysChem.* 2002; **7**: 630.
13. Cheng J-X, Potma EO, Xie XS. *J. Phys. Chem. A* 2002; **106**: 8561.
14. Schaller RD, Ziegelbauer J, Lee LF, Haber LH, Saykally RJ. *J. Phys. Chem. B* 2002; **106**: 8489.
15. Dudovich N, Oron D, Silberberg Y. *Nature (London)* 2002; **418**: 512.
16. Thompson TE, Tillack TW. *Annu. Rev. Biophys. Biophys. Chem.* 1985; **14**: 361.
17. Cotter TM, Kim JH, Chumanov GD. *J. Raman Spectrosc.* 1991; **22**: 729.
18. Cremer PS, Boxer SG. *J. Phys. Chem. B* 1999; **103**: 2554.
19. Akashi KI, Miyata H, Itoh H, Kinosita K. *Biophys. J.* 1996; **71**: 3242.
20. Nardi J, Bruinsma R, Sackmann E. *Phys. Rev. E* 1998; **58**: 6340.
21. Kloboucek A, Behrisch A, Faix J, Sackmann E. *Biophys. J.* 1999; **77**: 2311.
22. Guck J, Ananthakrishnan R, Mahmood H, Moon TJ, Cunningham CC, Käs J. *Biophys. J.* 2001; **81**: 767.
23. Jones DJ, Potma EO, Cheng J-X, Burfeindt B, Pang Y, Ye J, Xie XS. *Rev. Sci. Instrum.* 2002; **73**: 2843.
24. Cheng J-X, Volkmer A, Xie XS. *J. Opt. Soc. Am. B* 2002; **19**: 1363.
25. Levenson MD, Bloembergen N. *Phys. Rev. B* 1974; **10**: 4447.
26. Rand RP, Parsegian VA. *Biochim. Biophys. Acta* 1989; **988**: 352.
27. Curtis ASG. *J. Cell Biol.* 1964; **20**: 199.
28. Cheng J-X, Pautot S, Weitz DA, Xie XS. *Proc. Natl. Acad. Sci. USA* 2003; **100**: 9826.

APPENDIX 1

The CARS spectrum

To describe the CARS spectrum, both resonant and non-resonant signal contributions from the sample have to be taken into consideration. Whereas the non-resonant $\chi^{(3)}_{\text{glass}}$ is real and virtually independent of frequency, the nonlinear susceptibility from the lipids contains both resonant and nonresonant contributions:

$$\chi^{(3)}_{\text{lipid}} = \chi^{(3)}_{\text{NR,lipid}} + \chi^{(3)}_{\text{R,lipid}}(\omega_{\text{P}} - \omega_{\text{S}}) \tag{A1}$$

The resonant $\chi^{(3)}_{\text{R,lipid}}(\omega_{\text{P}} - \omega_{\text{S}})$ is complex and varies with the frequency difference between the pump and Stokes beams. It can be modeled according to

$$\chi^{(3)}_{\text{R,lipid}}(\omega_{\text{P}} - \omega_{\text{S}}) \propto \sum_k \frac{a_k}{\Omega_k - \omega_{\text{P}} + \omega_{\text{S}} - i\Gamma_k} \tag{A2}$$

with Ω_k the vibrational resonance of mode k with strength a_k and Γ_k the half-width of the vibrational band. Whereas the Raman spectrum is related to the imaginary part of the nonlinear susceptibility

$$I_{\text{Raman}}(\omega) \propto \text{Im}\{\chi^{(3)}_{\text{R,lipid}}(\omega)\} \tag{A3}$$

the CARS spectrum depends on both the real and imaginary parts. Owing to the different spectral behavior of the real and imaginary parts of $\chi^{(3)}_{\text{lipid}}$, the CARS field generated from the lipids acquires a frequency-dependent phase. Upon interference with the frequency-independent field of the non-resonant background, the characteristic dispersive CARS spectral lineshape is obtained. In order to account for the mixing contribution from the backreflected field from the coverslip in E-CARS, spectra are fitted to the following function:

$$I_{\text{CARS}} \propto |\chi^{(3)}_{\text{NR,glass}}|^2 + 2\varepsilon\chi^{(3)}_{\text{NR,glass}}\text{Re}\{\chi^{(3)}_{\text{R,lipid}}\} + |\chi^{(3)}_{\text{R,lipid}}|^2 \tag{A4}$$

Here it is assumed that $\chi^{(3)}_{\text{NR,glass}} >> \chi^{(3)}_{\text{NR,lipid}}$. The scaling parameter ε takes into account the efficiency of mixing of the nonresonant glass field with the lipid emission field.

APPENDIX 2

Imaging properties

To describe the CARS images from lipid bilayers in the vicinity of the glass coverslip, a model is required that takes into account the coherent spatial addition of the radiation field. Our starting point is the theory developed by Cheng *et al*.[24] To simplify the description, the following approximations are made. First, it is assumed that the excitation field $A(\mathbf{r})$ can be modeled with a Gaussian profile:

$$A(\mathbf{r}) = A_0 \exp\left[-\frac{2(x^2+y^2)}{r_0^2} - \frac{2z^2}{z_0^2}\right] \tag{A5}$$

where r_0 and z_0 are the lateral and axial widths, as defined by the e^{-2} points, respectively. The amplitude is described by A_0 and is proportional to $E_{\text{P}}^2 E_{\text{S}}^*$, where E_{P} and E_{S} are the pump and Stokes field, respectively. Second, aberrations of the excitation field due to the refractive index mismatch at the interface are ignored. Third, the Gouy phase shift of the focused field is neglected in our modeling. It has been shown previously that the Gouy phase shift has a negligible effect on the generated CARS signal field.[24] Finally, material dispersion effects are assumed to be small in the wavelength region of interest, which implies that $2k_{\text{P}} - k_{\text{S}} \approx k_{\text{CARS}}$.

In CARS, the pump and Stokes laser beams drive a nonlinear polarization $P^{(3)}(\mathbf{r})$ at a given point $\mathbf{r}$ in the sample. For pump and probe beams linearly polarized along x, the induced polarization is predominantly oriented along the x-axis and can be written as

$$P_x^{(3)}(\mathbf{r}) = 3\chi^{(3)}(\omega, \mathbf{r})A(\mathbf{r})\exp(ik_{\text{CARS}}z) \tag{A6}$$

where $\chi^{(3)}(\omega, \mathbf{r})$ is the third-order non-linear susceptibility of the sample. The non-linear polarization gives rise to a radiation field that is subsequently detected in the far-field. At a given point $\mathbf{R}$ in the far-field (Fig. 1), the total CARS radiation field is obtained by integrating the non-linear polarization over the microscopic volume V :[24]

$$E_{\text{CARS}}(\mathbf{R}) = \frac{\omega_{\text{CARS}}^2}{c^2}\frac{\exp(ik_{\text{CARS}}|\mathbf{R}|)}{|\mathbf{R}|}\int_V \eta(\mathbf{r})\exp(-ik_{\text{CARS}}\mathbf{n}\cdot\mathbf{r}) \times \mathbf{M}(\theta,\phi)P_x^{(3)}(\mathbf{r})\text{d}V \tag{A7}$$

Copyright © 2003 John Wiley & Sons, Ltd.

JRS

where $\eta(\mathbf{r})$ is the density of scatterers. The phase vector $\exp(-ik_{\mathrm{CARS}}\mathbf{n}\cdot\mathbf{r})$, with unit vector $\mathbf{n}$ in the direction of $\mathbf{R}$, accounts for the phase difference of different points in V with respect to $\mathbf{R}$. The projection vector $\mathbf{M}$ transforms the Cartesian components of $P_x^{(3)}(\mathbf{r})$ onto a spherical surface defined by θ, the angle of $\mathbf{R}$ with the optical axis, and the polar angleϕ, and is given by

$$\mathbf{M}(\theta,\phi) = \cos\theta\cos\phi\mathbf{i}_\theta - \sin\phi\mathbf{i}_\phi \tag{A8}$$

where $\mathbf{i}_\theta$ and $\mathbf{i}_\phi$ are the unit vectors in the directions of θ and ϕ, respectively. The total detected CARS intensity is obtained by integrating the modulus square of the CARS field over the full solid angle of the collimating objective lens:

$$I_{\mathrm{CARS}} \propto \int_{\theta_1}^{\theta_2} \mathrm{d}\theta \int_0^{2\pi} \mathrm{d}\phi |E_{\mathrm{CARS}}(\mathbf{R})|^2 R^2 \sin\theta \tag{A9}$$

In the studies presented in this paper, planar bilayers are scanned axially through focus. By substituting Eqns (A6) and (A8) into Eqn (A7), the signal intensity for the z-scan in E-CARS can be found as

$$S_{\mathrm{E-CARS}}(z) \propto A_0^2 \int_{\pi-\theta_{\max}}^{\pi} (1+\cos^2\theta)\exp\left(-\frac{k_{\mathrm{CARS}}^2 r_0^2}{4}\sin^2\theta\right) \times |F(\theta,z)|^2 \sin\theta \mathrm{d}\theta \tag{A10}$$

where $\theta_{\max}$ is the acceptance angle of the objective lens and the field function $F(\theta, z)$ is given by

$$F(\theta,z) = O(z) \otimes H(\theta,z) \tag{A11}$$

with

$$O(z) = \eta(z)\chi^{(3)}(\omega, z)$$

$$H(\theta,z) = \exp(-2z^2/z_0^2)\exp[ik_{\mathrm{CARS}}z(1-\cos\theta)]$$

The function $F(\theta, z)$ is a convolution of the object function $O(z)$ with the excitation field $H(\theta, z)$ along the axial coordinate. This expression bears much resemblance to the convolution relation between the object and the pointspread function in a confocal microscope, with the important exception that the CARS signal is modulated by an angular dependent phase mismatch function. For small angles θ, this phase function vanishes, whereas at larger angles the phase mismatch is more significant. It can be easily seen that there is a large phase mismatch of $-2k_{\mathrm{CARS}}z$ along the optical axis in the epi-direction ($\theta = \pi$), which gives rise to the almost complete cancellation of signal from the solvent/substrate bulk in E-CARS microscopy.

APPENDIX 3

Interference between surfaces

For a planar lipid bilayer on a glass coverslip, the signal in the epi-direction is composed of the CARS signal from the lipid layer and the forward going non-resonant signal from the glass that is back-reflected from the coverslip. Taking into account the phase shift of the signal from the glass upon back-reflection, the function $F(\theta, z)$can be written as

$$F(\theta,z) = F_{\mathrm{glass}}(\theta,z) + F_{\mathrm{lipid}}(\theta,z) \tag{A12}$$

with

$$F_{\mathrm{glass}}(\theta,z) = \exp(-2ik_{\mathrm{CARS}}z\cos\theta)\int_{-\infty}^{\infty}\eta_{\mathrm{glass}}\chi^{(3)}_{\mathrm{glass}}(z'-z)r_{\mathrm{Fr}} \times \exp\left(\frac{-2z'^2}{z_0^2}\right)\exp[ik_{\mathrm{CARS}}z'(1+\cos\theta)]\mathrm{d}z'$$

$$F_{\mathrm{lipid}}(\theta,z) = N_{\mathrm{lipid}}\chi^{(3)}_{\mathrm{lipid}}(\omega,\Delta z)\exp\left[\frac{-2(z+\Delta z)^2}{z_0^2}\right] \times \exp[ik_{\mathrm{CARS}}(1-\cos\theta)(z+\Delta z)]$$

where r_{Fr} denotes the Fresnel field reflection coefficient, N_{lipid} the number of scatterers in the lipid bilayer in the focal volume and Δz is the distance between the glass surface and the lipid bilayer. For strongly focused beams r_{Fr} depends on both θ and ϕ. Under the condition that angles θ larger than the critical angle for total internal reflection are discarded, r_{Fr} can be assumed a constant without affecting the profiles predicted by Eqn (A10) qualitatively. For glass/water interfaces, total internal reflectance can be effectively ignored for NAs below 1.4.

It can be seen by substituting Eqn (A12) into Eqn (A10) that the signal includes product terms of the field from the glass with the field from the lipid layer, which are proportional to $N_{\mathrm{glass}}N_{\mathrm{lipid}}\chi^{(3)}_{\mathrm{glass}}\chi^{(3)}_{\mathrm{lipid}}$. Depending on the relative phase of the two fields, these mixing contributions add a modulation to the CARS signal that can amplify or diminish the total signal yield. Upon tuning the distance Δz, a relative phase difference is introduced that is roughly proportional to $2k_{\mathrm{CARS}}\Delta z$. Hence an oscillatory signal is expected when Δz is changed linearly. In the case of a second bilayer located at the glass surface, Eqn (A12) is supplemented with an additional function $F_{\mathrm{lipid}}(\theta, z; \Delta z = 0)$.

Copyright © 2003 John Wiley & Sons, Ltd.